Combined label-free optical and optoacoustic imaging of model organisms at mesoscopy and microscopy resolutions

Dominik Soliman[a,b,†], George J. Tserevelakis[c,†], Murad Omar[a,b], Vasilis Ntziachristos[a,b,*]

[a]Institute for Biological and Medical Imaging (IBMI), Helmholtz Zentrum München, Neuherberg, Germany;
[b]Chair for Biological Imaging, Technische Universität München (TUM), Munich, Germany;
[c]Institute of Electronic Structure and Laser, Foundation for Research and Technology, Crete, Greece

ABSTRACT

We present a multi-scale imaging system that integrates five optoacoustic and multi-photon modalities into the same device. The hybrid microscope offers a unique zoom-in ability by allowing for optoacoustic microscopy and mesoscopy scans of the sample within the same imaging framework. Furthermore, by combining several label-free modalities, we are able to visualize a broad range of anatomical features, taking advantage of their complementary contrast mechanisms. We characterize the spatial resolution and relative orientation of the different sub-modalities and demonstrate the system's performance by the imaging of several model organisms *ex vivo*. The presented ability to dynamically vary scanning volume and resolution together with its multi-contrast and label-free imaging capabilities make the hybrid microscope a promising tool for comprehensive biological imaging.

Keywords: Photoacoustic microscopy; Optoacoustic microscopy; Multiphoton microscopy; Mesoscopy; Multi-modal imaging; Multi-scale imaging

1. INTRODUCTION

Since the dawn of optical microscopy, the ballistic nature of light has been persistently limiting its application for biological imaging to superficial tissues or thin samples [1]. On the other hand, the investigation of organ and whole-organism level processes requires a larger field of view (FOV) and higher penetration depth. During the previous years, several mesoscopic imaging approaches have been developed to overcome this challenge, including mesoscopic fluorescence tomography (MFT) [2] and mesoscopic optoacoustic imaging [3-5]. Additionally, our group has recently introduced raster-scan optoacoustic mesoscopy (RSOM) in an epi-illumination configuration, which achieves a lateral and axial resolution of ~20 μm and ~4 μm, respectively, up to a depth of 3 mm [6]. However, these approaches lack the high spatial resolution required for investigating cellular and sub-cellular structures and processes. Furthermore, in order to gain a comprehensive understanding of biological organisms, multi-modal imaging is superior to utilizing a single contrast mechanism in terms of simultaneously visualizing a broad range of features. In optoacoustic microscopy, multi-modal imaging has been achieved in different implementations [7-9]. However, concurrent multi-scale imaging has not been demonstrated. Finally, label-free imaging constitutes an important advantage over techniques that rely on staining, such as MFT or confocal microscopy, which can potentially be toxic for biological samples [10].

In this work, we present a multi-modal microscopy system that operates at different geometrical scales by combining microscopic and mesoscopic modes into the same imaging framework. In particular, the developed hybrid device combines raster-scan optoacoustic mesoscopy (RSOM) with optoacoustic (OM), two-photon excitation fluorescence (TPEF), second-harmonic generation (SHG) and third-harmonic generation (THG) microscopy. The system allows for scanning two orders of magnitude larger fields of view compared to standard microscopy and achieves imaging depths of several millimeters. Through the separate reconstruction of different frequency bands, the broadband nature of optoacoustic signals can be utilized to achieve multi-scale imaging with RSOM within a single scanning volume [11]. The full zoom-in ability arises from the combination with the microscopy modalities, which allows for a dynamic FOV selection within the sample. At the same time, multi-modal label-free imaging enables the concurrent visualization of various biological features with complementary contrast. The spatial resolution of the system and the relative orientation of scanning volumes is characterized via phantoms. Subsequently, we showcase the unique multi-scale and multi-contrast imaging performance of the hybrid microscope by the *ex vivo* imaging of zebrafish larvae and a mouse ear.

[†]These authors contributed equally to this work

*v.ntziachristos@tum.de

Photons Plus Ultrasound: Imaging and Sensing 2016, edited by Alexander A. Oraevsky, Lihong V. Wang
Proc. of SPIE Vol. 9708, 97083B · © 2016 SPIE · CCC code: 1605-7422/16/$18 · doi: 10.1117/12.2208861

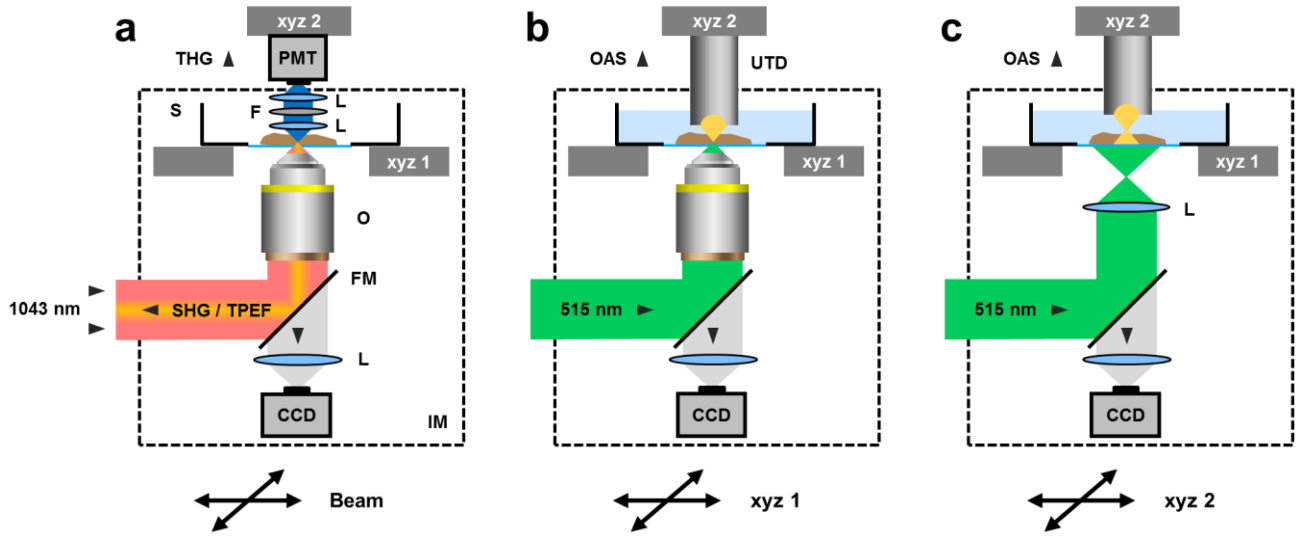

Figure 1. Schematic of the IMMSOM system. The different scanning configurations are illustrated for (a) multiphoton microscopy, (b) optoacoustic microscopy and (c) optoacoustic mesoscopy. The arrows at the bottom denote the part that is moved for scanning in the respective modes. Abbreviations: (IM) Inverted microscope. (xyz) Motorized xyz-stage. (O) Objective. (L) Lens. (F) Optical filter. (FM) Flip-mount mirror. (S) Sample holder. (PMT) Photomultiplier tube. (UTD) Ultrasound transducer. (OAS) Optoacoustic signal.

2. METHODS

2.1 Experimental setup

The central part of the integrated multiphoton and multi-scale optoacoustic microscope (IMMSOM), as well as the different scanning modes are illustrated by Figure 1. A detailed description of the optical and acquisition systems is given in [12]. The sample is mounted on a glass bottom petri dish, which is placed on a motorized xyz-stage (MLS203 2 and MZS500 E, Thorlabs, Newton, NJ, USA) on top of a modified inverted microscope (AxioObserver.D1, Zeiss, Jena, Germany). A CCD camera (AxioCam ICc 1, Zeiss, Jena, Germany) is used to perform brightfield microscopy for orientation and reference purposes.

For multiphoton microscopy (see Figure 1(a)), a femtosecond laser (YBIX, Time-Bandwidth, Zurich, Switzerland) with a wavelength of 1043 nm, 170 fs pulse width and a repetition rate of 84.4 MHz is focused into the sample by a 10X objective (Plan Apochromat 10X, Zeiss, Jena, Germany; Numerical aperture: 0.45). In case of SHG and TPEF imaging, the non-linear signals originating from the laser focus are recorded in backward direction by a photomultiplier (PMT) (H9305 03, Hamamatsu, Hamamatsu City, Japan). For THG microscopy, the mainly in forward direction emitted signals are collected in transmission mode by a second PMT. Images are recorded by scanning the focus inside the sample by means of a set of galvanometric mirrors (6215H, Cambridge Technology, Bedford, Massachusetts, USA).

The optoacoustic modalities employ a nanosecond laser (Flare HP PQ Green 2k 500, Innolight GmbH, Hannover, Germany) with a wavelength of 515 nm, 1.8 ns pulse width and a repetition rate of 1.2 kHz. The optoacoustic signals are detected via a spherically focused 78 MHz transducer (SONAXIS, Besancon, France; bandwidth: ~25–125 MHz) in transmission mode, which can be interchanged with the PMT for THG imaging. Figure 1(b) depicts the scanning mode for optoacoustic microscopy. Transducer and illumination are in a fixed confocal and coaxial arrangement and the same objective is employed to focus the attenuated laser beam. The sample holder is filled with water for acoustic coupling. The microscope xyz-stage is used to translate the sample laterally in discrete steps. At every position, the time-resolved optoacoustic signals are recorded and averaged 20 times. On the other hand, for RSOM, the entire sample is illuminated by the unattenuated laser, using a lens instead of the objective (see Figure 1(c)). For scanning, sample and illumination remain stationary, while the transducer is raster-scanned laterally above the sample in the positive defocus by another motorized xyz-stage (M 683.2U4 and M 501.1DG, Physik Instrumente GmbH & Co. KG, Karlsruhe, Germany). This stage is also used to position transducer and PMT for microscopy scans.

2.2 Reconstruction and image processing

All optoacoustic signals were bandpass filtered in the transducer's sensitivity range of 25-125 MHz in order to reject noise. For OM, the Hilbert transform was employed to calculate the signal's envelopes. In the case of RSOM, tomographic image reconstruction was used. More specifically, we employed a 3D filtered backprojection algorithm running on a GPU. Prior to the reconstruction, we applied a spatial high-pass filter on the raw data to remove acoustic signals arising from laser reflections, which appeared always at the same time points in each A-scan. In order to take the sensitivity field of the transducer into account, we weighted the signals with a 3D hyperboloid that had a Gaussian cross-section. Since the transducer's sensitivity field depends on the measured frequencies, we adapted the dimensions of the hyperboloid to the reconstructed frequency bands. The reconstruction voxel size was 5 µm × 5 µm × 2.5 µm. As a last step, the reconstructed volume was weighted with a 2D-Gaussian along the xy-dimensions in order to correct for an uneven illumination with the Gaussian-shaped laser beam cone.

Final co-registration and image processing was done with imageJ and involved standard procedures, such as median filtering, windowing, interpolation and smoothing, which were applied to the entire images. For the RSOM vasculature image, we employed a 2D Frangi vesselness filter [13] with different scales for the images representing the two separately reconstructed frequency bands in order to enhance the visibility of small vessels.

2.3 Spatial resolution characterization and co-registration

The spatial resolution of the OM modality was determined by the imaging of a single 954 nm black polystyrene microsphere (Polybead, Polysciences Inc., Warrington, Pennsylvania) in 0.2 µm steps with a pulse energy of ~12 nJ. The axial resolution was provided by the full width at half maximum (FWHM) of the axial profile of the sphere, while we estimated the lateral resolution following a deconvolution of the measured profile with the known sphere diameter.

In order to characterize the resolution of the multiphoton modalities, we imaged a single 100 nm fluorescent nanobead (TetraSpeck Fluorescent Microspheres Size Kit, Invitrogen, Carlsbad, California, USA), which represented a point source and thus directly yielded the lateral resolution. The axial resolution was determined by performing a z-scan across the upper glass-air-interface of a coverslip in 0.5 µm steps. The FWHM of the resulting profile represented the axial resolution of the multiphoton modalities.

The co-registration of the volumes scanned with the different modalities was addressed by imaging an 18 µm suture cross phantom with each sub-system and finding the mutual lateral and axial offsets. These offsets were corrected prior to each scan with the respective modalities via the xyz-stages.

2.4 Multi-scale zebrafish imaging

To demonstrate the multi-scale capabilities of IMMSOM, we imaged a 5-days-old wildtype zebrafish larva *ex vivo* with the optoacoustic modalities. The specimen was covered with ultrasound gel and fixed on a glass bottom dish with plastic foil. For the RSOM scan, a FOV of 3 mm × 3 mm was scanned with a step size of 4 µm. The subsequent OM scan was performed at the tail of the larva within a 300 µm × 300 µm region using a step size of 1.5 µm. The laser energy at the sample was measured to be ~13 nJ per pulse.

2.5 Hybrid imaging of model organisms

We subsequently went a step further and investigated the full multi-scale and multi-contrast performance of the system by the hybrid imaging of a 6-days-old zebrafish larva and a mouse ear *ex vivo*. The zebrafish was first scanned with RSOM in a 4 mm × 4 mm FOV and a 5 µm step size. Two frequency bands were selected for multi-frequency reconstruction, the full detection bandwidth of 25-125 MHz and the high-frequency band of 75-125 MHz. The following microscopy scans were performed in a 315 µm × 315 µm region at the tail. In case of OM, the step size was 1.8 µm and the pulse energy at the sample was ~8 nJ. For multiphoton microscopy, the pulse energy of the fs laser at the focus was ~0.5 nJ and the pixel size was ~0.5 µm. The images were recorded through a depth of 50 µm with a step size of 2 µm and averaged thirty times to improve the signal-to-noise ratio (SNR).

The mouse ear was excised and fixed in agar inside a glass bottom petri dish. The RSOM measurement covered a 2 mm × 2 mm region using a step size of 3 µm. Similar to the zebrafish measurement, we reconstructed the full bandwidth and the high-frequency band. Next, a FOV of 375 µm × 375 µm was selected for microscopy scans at the branching of a big vessel. OM was performed with a step size of 1.8 µm and a pulse energy of ~85 nJ. To increase the SNR, forty averages were recorded per pixel. Multiphoton scans were performed through a depth of 50 µm with 2 µm steps and averaged twenty times. The energy per pulse was set to ~1.3 nJ.

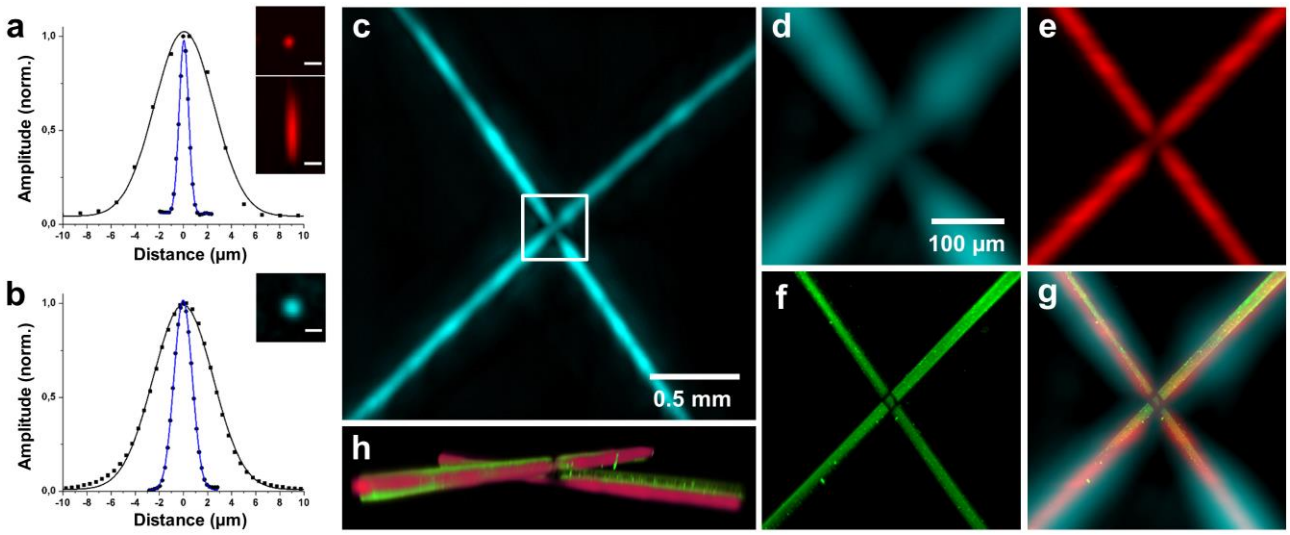

Figure 2. Spatial resolution and offset characterization of the IMMSOM modalities. (a-b) Resolution characterization. (a) OM imaging of a 954 nm microsphere. The graphs show the lateral (blue) and axial (black) profiles of the sphere fitted with Gaussian curves. The insets illustrate lateral and axial views of the microsphere. (b) Multiphoton microscope. The blue curve represents the Gaussian fit of the lateral profile of a 100 nm bead. The inset shows the corresponding top view of the TPEF imaged bead, representing the lateral point spread function. The black curve represents the THG z-scan across the upper glass-air interface of a coverslip. Scale bars: 2 µm. (c-h) Multi-modal imaging of an 18 µm suture cross phantom after correction of the mutual spatial offsets. (c) RSOM scan. The white box indicates the FOV of microscopy scans. (d) Zoom into the white square in the RSOM image. (e) OM scan. (f) THG image. (g) Overlay of RSOM, OM and THG scans. (h) Overlay of the OM (red color) and THG (green color) 3D reconstructions of the suture cross phantom.

3. RESULTS

3.1 Spatial resolution characterization and co-registration

Figure 2(a) shows the lateral (blue curve) and axial (black curve) Gaussian fitted profiles through the microsphere imaged with OM, yielding a lateral and axial resolution of 0.83 µm and 5.78 µm, respectively. Maximum amplitude projections (MAP) of the sphere in top and side view are depicted by the insets. Concerning RSOM, the lateral resolution depends on the specifications of the used transducer and has previously been demonstrated to be ~20 µm up to a depth of 3 mm [14], whereas the axial resolution is identical to OM and is also governed by the transducer properties.

The spatial resolution characterization of the multiphoton microscope is illustrated in Figure 2(b). From the lateral profile (blue curve) of the nanobead measured through TPEF imaging, the FWHM and thus the lateral resolution of the multiphoton modalities was found to be 1.75 µm. The factor of ~2 compared to the OM resolution originated mainly from the two times larger wavelength of the employed fs laser. A top-view image of the nanobead is provided by the inset. The black curve illustrates the THG measurement across the coverslip's upper glass-air interface, which yielded an axial resolution of 5.84 µm.

Figure 2(c-h) depicts the multi-modal imaging of the suture cross phantom after spatial offset correction. Figure 2(c) shows the RSOM scan of an extended FOV of the phantom. The white box indicates the region of subsequent microscopy scans. Figure 2(d) shows a zoom into this region of the RSOM image. OM and THG scans of the same FOV are illustrated in Figure 2(e) and 2(f), respectively. The difference in lateral resolution between OM and RSOM is reflected by the larger diameter of the imaged sutures in Figure 2(d). An overlay of the RSOM, OM and THG scans is shown in Figure 2(g), demonstrating that the different FOVs can precisely be co-registered and the orientation of the imaged sample is preserved in all measurements. A 3D reconstruction overlay of the OM (red color) and THG (green color) scans of the suture cross is illustrated in Figure 2(h), validating that co-registration is also achieved along the depth dimension.

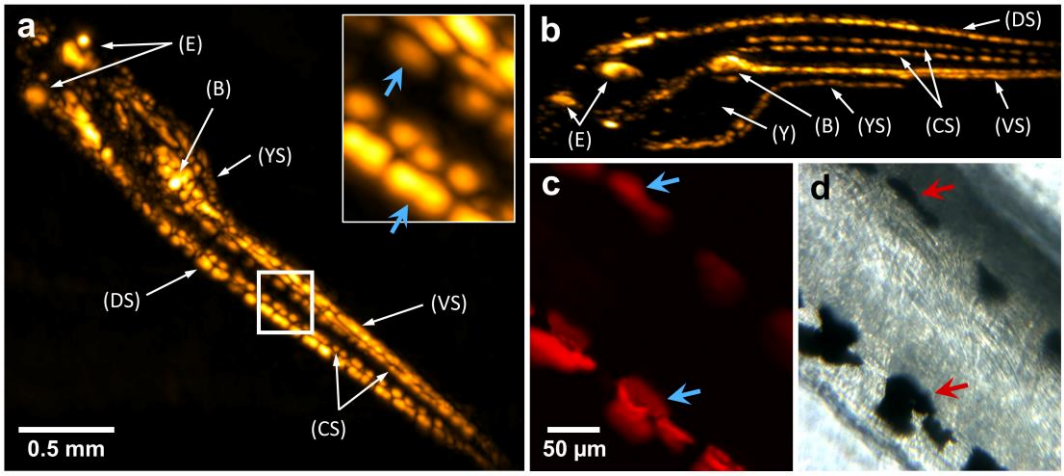

Figure 3. Multi-scale optoacoustic imaging of a wildtype zebrafish larva *ex vivo*. (a-b) RSOM scan of the entire fish. Maximum amplitude projections (MAP) are shown in top view (a) and 65° side-view (b). The eyes (E), yolk (Y), swim bladder (B), as well as melanocyte patterns forming the yolk sac stripe (YS), ventral stripe (VS), dorsal stripe (DS) and central stripes (CS) can be identified. The white box in (a) indicates the region of subsequent high-resolution scans with optoacoustic (c) and brightfield (d) microscopy. The inset in (a) shows a zoom of the FOV in the white box for comparison. Two exemplary melanophores are marked with blue and red arrows throughout the images.

3.2 Multi-scale zebrafish imaging

Figure 3 illustrates the multi-scale imaging of a 5-days-old zebrafish larva *ex vivo* using the optoacoustic modalities. A z-projection of the RSOM scan covering the whole fish is shown in Figure 3(a). A side-view MAP from a 65° angle is shown in Figure 3(b). In the two RSOM images, the eyes (E), yolk (Y), swim bladder (B), and the melanocyte patterns along the body and tail forming the yolk sac stripe (YS), ventral stripe (VS), dorsal stripe (DS) and central stripes (CS) can be identified. A FOV at the tail of the fish indicated by the white box in Figure 3(a) was selected for the high-resolution OM scan. The inset in Figure 3(a) illustrates a zoom into the region enclosed by the box. OM and brightfield microscopy images of this region are shown in Figure 3(c) and 3(d), respectively, and visualize single melanocytes of the dorsal (lower stripe) and central (upper stripe) melanophore stripes. The blue and red arrows mark the same two exemplary melanocytes throughout the images for comparison.

3.3 Hybrid imaging of model organisms

In Figure 4, the multi-scale and multi-contrast imaging of two model organisms is showcased, an excised mouse ear (Figure 4(a-d)) and a 6-days-old wildtype zebrafish larva *ex vivo* (Figure 4(e-h)).

The RSOM scan of the mouse ear is shown in Figure 4(a), visualizing the vasculature of the ear. The white box marks the selected FOV for the microscopy scans. In Figure 4(b), two vesselness filtered reconstructions using the full frequency range (red color) and the high frequencies (cyan color) are overlaid. Through the separate reconstruction, small vessels and structures emerged from the low-frequency noise, which usually has a higher amplitude and covers the fine details. This effect is illustrated by the insets in Figure 4(a) and 4(b), which represent magnifications of the region indicated by the dashed white boxes. In the multi-frequency reconstruction, several small vessels are clearly visible that are obscured in the respective inset in Figure 4(a). In Figure 4(c), an overlay of the subsequent high-resolution scans with OM (red color, branching vessel), SHG (blue color, collagen in the dermis layer) and THG (green color, keratinocytes in the epidermis and hair follicles) is shown. For comparison, a brightfield image is provided in Figure 4(d).

This imaging procedure was repeated for the zebrafish larva. Figure 4(e) illustrates the RSOM scan of the whole specimen, visualizing the same features as discussed in the previous section. The multi-frequency reconstruction is depicted in Figure 4(f). As can be seen from the two insets, representing magnifications of the region highlighted by the two white dashed boxes, several small features and structures are apparent in the multi-frequency image, which are not observed in standard reconstruction. Two prominent examples are marked by the white arrows. The solid white square in

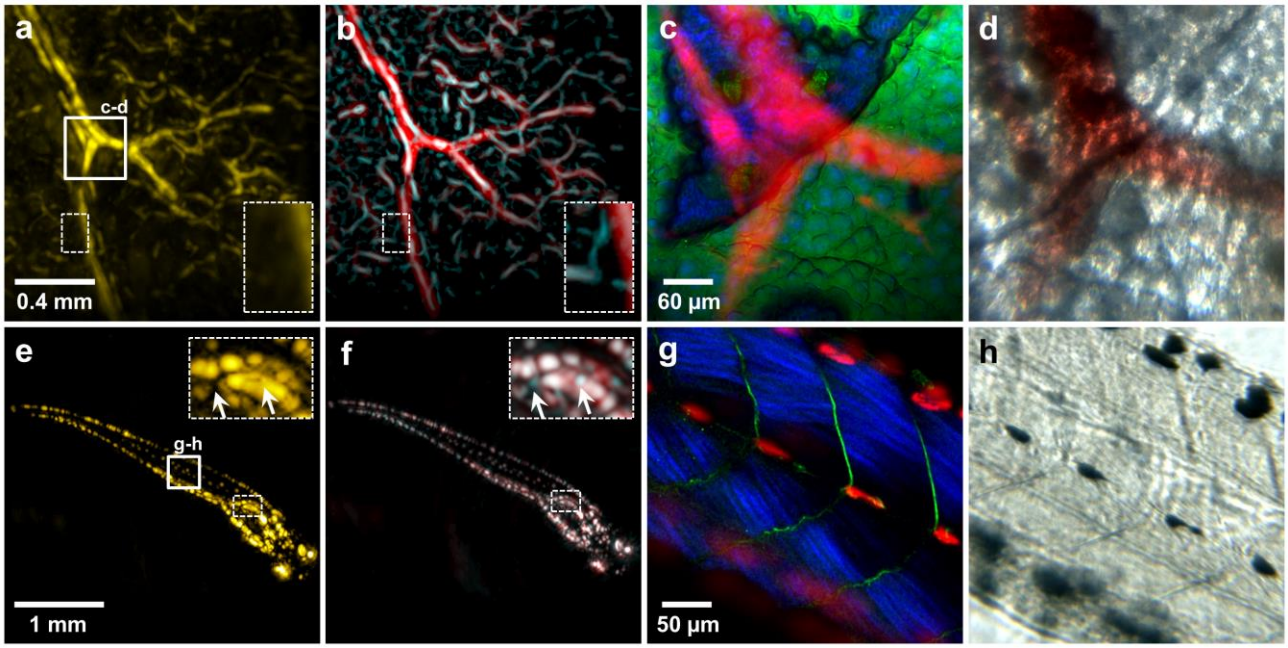

Figure 4. Hybrid imaging of a mouse ear (a-d) and a zebrafish larva (e-h) *ex vivo*. (a) RSOM scan of an extended region of the ear. (b) Multi-frequency reconstruction of the RSOM scan showing an overlay of all (red) and high (cyan) frequencies. Insets show magnified regions indicated by the dashed white boxes. (c) Microscopy scans in the area indicated by the solid white box in (a), showing an overlay of OM (red), SHG (blue) and THG (green) images. (d) Brightfield image the same region. (e) RSOM scan of the zebrafish larva. (f) Multi-frequency reconstruction of the RSOM scan showing an overlay of all (red) and high (cyan) frequencies. The insets show magnified regions indicated by the dashed white boxes. (g) Microscopy scans at the fish trunk as indicated by the solid white box in (e), showing an overlay of OM (red), SHG (blue) and THG (green) images. (h) Brightfield image of the same region.

Figure 4(e) indicates the FOV selected for microscopy scans. Figure 4(g) shows the OM (red color, single melanocytes), SHG (blue color, fish musculature) and THG (green color, connective tissue) scans as an overlay. The reference brightfield image is depicted in Figure 4(h).

4. DISCUSSION

The presented integrated multiphoton and multi-scale optoacoustic microscope (IMMSOM) has been demonstrated to provide a unique combination of dynamic scanning volume and resolution selection with multi-contrast imaging capabilities without the necessity of staining. The hybrid imaging of a suture cross phantom (see Figure 2) showcased the ability to precisely co-align the volumes scanned by the different sub-modalities in 3D.

By the concurrent mesoscopic and microscopic optoacoustic imaging of a zebrafish larva *ex vivo* (see Figure 3), the multi-scale capabilities of the system were researched. This implementation combines advantages of both methodologies. The whole body distribution of pigments is captured by RSOM with a resolution high enough to visualize single melanophores. On the other hand, images of single melanocytes with sub-cellular resolution and high contrast are provided by the OM modality, which, however, can only visualize cells within the relatively thin optical focal plane. This is evident from the OM and brightfield images, which only show two pigment stripes, whereas the other stripes are out of focus.

Finally, the full performance of the developed hybrid device was demonstrated by the multi-scale and multi-modal imaging of a mouse ear and another zebrafish larva *ex vivo* (see Figure 4). We showcased the inherent multi-scale nature of the RSOM modality by performing a multi-frequency analysis of both specimens. By applying separate vesselness filters on the two reconstructions of the mouse ear, we were able to visualize small vasculature otherwise hidden in low-

frequency noise. Through the subsequent multi-modal microscopy imaging, we could concurrently visualize blood vessels, keratinocytes and hair follicles in the epidermis, as well as collagen in the extracellular matrix of the ear. In case of the zebrafish larva, we simultaneously captured the musculature, resolving single muscle fibrils, the vertical myosepta connecting the different muscle segments, single melanocytes and the global pigment distribution of the fish.

In summary, the hybrid microscope presented in this work combines the realms of mesoscopic and microscopic imaging into a single device, offering the possibility to scan entire specimens or large structures with high resolution and to dynamically zoom into interesting regions for imaging with sub-cellular resolution. The multi-contrast capabilities of the system, combining five different label-free modalities, enables the concurrent visualization of a large number of anatomical features, leading to new possibilities in biological imaging. A future implementation in epi-illumination mode could extend the application of IMMSOM to larger specimens.

ACKNOWLEDGEMENTS

The authors would like to thank Prof. Gil Westmeyer and Dr. Antonella Lauri for providing the zebrafish larvae. V.N. received funding from an ERC Senior Investigator Award, a DFG Koseleck Award, and the TUM Excellence Initiative.

REFERENCES

[1] Ntziachristos, V., "Going deeper than microscopy: The optical imaging frontier in biology," Nat. Methods 7(8), 603-614 (2010).
[2] Vinegoni, C., Pitsouli, C., Razansky, D., Perrimon, N. and Ntziachristos, V., "In vivo imaging of Drosophila melanogaster pupae with mesoscopic fluorescence tomography," Nat Methods 5(1), 45-47 (2008).
[3] Zhang, H. F., Maslov, K., Stoica, G. and Wang, L. V., "Functional photoacoustic microscopy for high-resolution and noninvasive in vivo imaging," Nat Biotechnol. 24(7), 848-851 (2006).
[4] Razansky, D., Distel, M., Vinegoni, C., Ma, R., Perrimon, N., Köster, R. W. and Ntziachristos, V., "Multispectral opto-acoustic tomography of deep-seated fluorescent proteins in vivo," Nat. Photonics 3(7), 412-417 (2009).
[5] Chekkoury, A., Gateau, J., Driessen, W., Symvoulidis, P., Bézière, N., Feuchtinger, A., Walch, A. and Ntziachristos, V., "Optical mesoscopy without the scatter: broadband multispectral optoacoustic mesoscopy," Biomed. Opt. Express, 6(9), 3134-3148 (2015).
[6] Omar, M., Soliman, D., Gateau, J. and Ntziachristos, V., "Ultrawideband reflection-mode optoacoustic mesoscopy," Opt. Lett. 39(13), 3911-3914 (2014).
[7] Tserevelakis, G. J., Soliman, D., Omar, M. and Ntziachristos, V., "Hybrid multiphoton and optoacoustic microscope," Opt. Lett. 39(7), 1819-1822 (2014).
[8] Rao, B., Soto, F., Kerschensteiner, D. and Wang, L. V., "Integrated photoacoustic, confocal and two-photon microscope," J. Biomed. Opt. 19(3), 036002 (2014).
[9] Jiao, S., Xie, Z., Zhang, H.F. and Puliafito, C. A., "Simultaneous multimodal imaging with integrated photoacoustic microscopy and optical coherence tomography," Opt. Lett. 34(19), 2961-2963 (2009).
[10] Ouédraogo, G. D. and Redmond, R. W., "Secondary Reactive Oxygen Species Extend the Range of Photosensitization Effects in Cells: DNA Damage Produced Via Initial Membrane Photosensitization," Photochem. Photobiol 77(2), 192-203 (2003).
[11] Omar, M., Schwarz, M., Soliman, D., Symvoulidis, P. and Ntziachristos, V., "Pushing the optical imaging limits of cancer with multi-frequency-band raster-scan optoacoustic mesoscopy (RSOM)," Neoplasia 17(2), 208-214 (2015).
[12] Soliman, D., Tserevelakis, G. J., Omar, M. and Ntziachristos, V., "Combining microscopy with mesoscopy using optical and optoacoustic label-free modes," Sci. Rep. 5, 12902 (2015).
[13] Frangi, A., Niessen, W., Vincken, K. and Viergever, M., "Multiscale vessel enhancement filtering," Image Computing and Computer-Assisted Intervention - MICCAI'98, W. Wells, A. Colchester, and S. Delp, eds., Lecture Notes in Computer Science, Springer Verlag, 1496, 130–137, (1998).
[14] Omar, M., Gateau, J. and Ntziachristos, V., "Raster-scan optoacoustic mesoscopy in the 25-125 MHz range," Opt. Lett. 38(14), 2472-2474 (2013).